AIP | Applied Physics Letters

Multiple Dirac points and perfect transmission in graphene with a dimerlike potential

Rui-Li Zhang, Han-Tian Gao, Yu Zhou, Ren-Hao Fan, Dong-Xiang Qi et al.

Citation: Appl. Phys. Lett. **103**, 121605 (2013); doi: 10.1063/1.4821943
View online: http://dx.doi.org/10.1063/1.4821943
View Table of Contents: http://apl.aip.org/resource/1/APPLAB/v103/i12
Published by the AIP Publishing LLC.

Multiple Dirac points and perfect transmission in graphene with a dimerlike potential

Rui-Li Zhang,[a] Han-Tian Gao, Yu Zhou, Ren-Hao Fan, Dong-Xiang Qi, Ru-Wen Peng,[a] Run-Sheng Huang, and Mu Wang
National Laboratory of Solid State Microstructures and Department of Physics, Nanjing University, Nanjing 210093, China

(Received 23 June 2013; accepted 6 September 2013; published online 19 September 2013)

In this work, we investigate electronic band structures and transport properties in dimerlike graphene superlattices (DGSLs), where the modulated potentials of square barrier A and well B on graphene are arranged as $S(m) = (AB)^m(BA)^m$. Here m is the repeated number of units. It is found that the mirror symmetry of the potential distribution on graphene can induce extra Dirac points (DPs), which originates from the dimerlike positional correlations in the system. The induced DPs, which are exactly located at the energy corresponding to zero averaged wave number, do not exist in the periodic graphene superlattices of $(AB)^m$. The number and the position of DPs in the zero averaged wave number gap of DGSL can be manipulated. Correspondingly, multiple perfect transmissions are observed at the resonant modes. Moreover, the conductance for DGSL presents extra resonant peaks accompanying with the emergence of the induced DPs. The investigations may have potential applications in graphene-based electronic devices. © *2013 AIP Publishing LLC*. [http://dx.doi.org/10.1063/1.4821943]

Since the experimental realization of graphene by Novoselov *et al.*,[1] considerable attention has been paid to the physical properties of the two-dimensional (2D) honeycomb lattice of carbon atoms.[2,3] In graphene, the low-energy charge carriers are well described by the 2D massless Dirac equation with the valence and conduction bands touching each other at the Dirac point (DP). Such characteristics offer exciting opportunities for the occurrence of unusual properties such as the half-integer quantum-Hall effect,[4] Klein tunneling, and so on.[5] The Klein tunneling in graphene, which has been observed in the experiment,[6] describes the perfect transmission of carriers through a single-barrier at normal incidence regardless of the height and the width of the barrier.[7] Basically, the electronic properties of semiconductor superlattices are different from those in a single-barrier junction. Therefore, the electronic properties for graphene in multiple barriers or periodic potentials, i.e., graphene superlattices (GSLs), may, in principle, be explored and exploited.

The GSLs can be fabricated by adsorbing adatoms on graphene surface, by positioning and aligning impurities with scanning tunneling microscopy or by applying a local top gate voltage to graphene.[8–11] Park *et al.* have demonstrated that the propagation of charge carriers through a graphene-based superlattice is highly anisotropic.[12] The anisotropic behavior has been predicted as a precursor of the formation of further DPs in the electronic energy dispersion relation of the system.[13] These Dirac fermions contribute to the degeneracy of Landau levels, and the unusual properties of quantum-Hall effect have been discovered in the system.[14] It has also been identified that the DPs exactly locate at the energy corresponding to the zero averaged wave number (zero-$\bar{k}$).[15] As an analog of photonic zero-$\bar{n}$ gap,[16] the zero-$\bar{k}$ gap is robust against the lattice constants and the structural disorder which can be used to control the electron transport in GSLs. Up to now, electronic band gaps and transport properties of GSLs in the presence of periodic,[17] Thue-Morse aperiodic,[18] Fibonacci quasi-periodic,[19] and disordered[20] potentials have been studied by several groups.

In this work, we study how the mirror symmetry[21–23] affects the electronic band structures and the transport properties in dimerlike graphene superlattices (DGSLs). It is shown that the internal symmetry can induce extra DPs in the zero-$\bar{k}$ gap of DGSLs. Correspondingly, multiple resonant transmissions are realized. The investigations may have potential applications in graphene-based electronic devices.

Consider a DGSL constructed as $S(m) = (AB)^m(BA)^m$, where m is the repeated number of units and element A (B) denotes the square potential barrier V_A (well V_B) with the width l_A (l_B). The DGSL locates at the x-y plane with the growth direction along the x-axis, and the electron is incident upon the system at an angle ϕ_i with respect to the x-axis. For charge carriers moving near the K point in a DGSL, the Hamiltonian[5] is given by

$$H = v_F \boldsymbol{\sigma}.\boldsymbol{p} + V(x)I, \tag{1}$$

where the Fermi velocity $v_F \approx 10^6$ m/s, I is the unit matrix, $\boldsymbol{\sigma} = (\sigma_x, \sigma_y)$ are the Pauli matrices of the pseudospin, $\boldsymbol{p} = (p_x, p_y)$ are the momentum operators, and $V(x) = V_A$ (V_B) in the barriers A (wells B). The electronic pseudospin wavefunctions at the input side and output side of A can be connected by the transfer matrix[15]

$$M_A = \frac{1}{\cos\phi_A}\begin{pmatrix} \cos(q_A l_A - \phi_A) & i\sin(q_A l_A) \\ i\sin(q_A l_A) & \cos(q_A l_A + \phi_A) \end{pmatrix}, \tag{2}$$

where $\phi_A = \arcsin(k_y/k_A)$ denotes the incident angle of carriers in A. Here $k_A = (E - V_A)/\hbar v_F$ is the wave vector inside

[a]Authors to whom correspondence should be addressed. Electronic addresses: rlzhang@nju.edu.cn and rwpeng@nju.edu.cn

the potential V_A, E is the incident energy of carriers, and k_y is the y component of k_A. While the x component of k_A can be expressed as $q_A = sign(k_A)\sqrt{k_A^2 - k_y^2}$ for $k_y^2 < k_A^2$, otherwise $q_A = i\sqrt{k_y^2 - k_A^2}$. When the carriers transport across B, the transfer matrix M_B has the same form as Eq. (2) by replacing the subscript A with B. Therefore, we can get the total transfer matrix M across the DGSL, relating the incident and reflection waves to the transmission wave. Then, the electronic transmission coefficient T can be obtained as

$$T = \left| \frac{2\cos\phi_i}{(M_{22}e^{-i\phi_i} + M_{11}e^{i\phi_e}) - M_{12}e^{i(\phi_e - \phi_i)} - M_{21}} \right|^2, \quad (3)$$

where ϕ_i (ϕ_e) is the angle between the incident (exit) direction of carriers and the x-axis at the input (output) side of DGSL, and $M_{ij}(i,j = 1,2)$ is the matrix element of M. Once the transmission coefficient is achieved, the conductance of the system at zero temperature can be obtained[24] by $G = G_0\int_0^{\pi/2} T\cos\phi_i d\phi_i$. Here $G_0 = 2e^2 m v_F L_y/\hbar^2$ with L_y denoting the length of the graphene stripe in the y direction. Moreover, the Fano factor[13] is given by $F = \int_{-\pi/2}^{\pi/2} T(1-T)\cos\phi_i d\phi_i / \int_{-\pi/2}^{\pi/2} T\cos\phi_i d\phi_i$.

Because the transport properties are ultimately determined by the energy spectra of the system, we first derive the electronic dispersion relation of DGSL. The simple structure for DGSL of $S(m) = (AB)^m(BA)^m$ with $m = 1$ is considered, and the value of m does not affect the DPs in the zero-$\bar{k}$ gap of the system. According to the Bloch's theorem, the electronic dispersion relation can be obtained by $2\cos(\alpha_x L) = Tr[M_A M_B M_B M_A]$, where L is the width of the unit cell. From the definition of zero-$\bar{k}$,[18] we can get the energy associated with the zero-$\bar{k}$ as $E = [V_A + (l_B/l_A) \times V_B]/(1 + l_B/l_A)$. By fixing the ratio $l_A/l_B = 1$, the relation between the incident angles of carriers in the barrier A and well B is obtained as $\phi_A = -\phi_B$. Then, the electronic dispersion relation becomes

$$\cos(\alpha_x L) = \cos[2q_A l_A + 2q_B l_B] + [\cos(2\phi_A) - 1]\sin(2q_A l_A) \times \sin(2q_B l_B)/\cos^2\phi_A. \quad (4)$$

This equation indicates that when $q_A l_A = -q_B l_B = n\pi/2$ ($n = 0, \pm 1, \cdots$), α_x has the real solutions. Otherwise, when $q_A l_A = -q_B l_B \neq n\pi/2$ and $\phi_A \neq 0$, α_x has not the real solution. That means there exist band gaps at the energy corresponding to the zero-$\bar{k}$, while the gap will be closed to form DPs in the zero-$\bar{k}$ gap of DGSL under the condition of $q_A l_A = -q_B l_B = n\pi/2$ ($n = 0, \pm 1, \cdots$). This condition can also be expressed as $k_{y,n} = \pm\sqrt{[V/(\hbar v_F)]^2 - (2n\pi/L)^2}$, where $V = (V_A - V_B)/2$ and $L = 2(l_A + l_B)$, respectively. Compared with that in the periodic graphene superlattices (PGSLs),[15] the width of unit cell L is doubled due to the mirror symmetry of "*ABBA*," which makes a dimerlike positional correlation in the DGSL. Consequently, extra DPs are obtained in the DGSL when the phase difference of incident waves across each element A (B) is a half-integer multiple of π.

In order to show that the mirror symmetry makes a "dimer" in the structure which finally induces the perfect transmission at the resonant modes in the DGSL, we consider the total transfer matrix M across the system of $S(m) = (AB)^m(BA)^m$. In the center of M, the pair of matrices related to the dimer "*BB*" is

$$M_{BB} = \frac{1}{1+\cos(2\phi_B)} \begin{pmatrix} \eta_+ & i2\sin(2q_B l_B)\cos\phi_B \\ i2\sin(2q_B l_B)\cos\phi_B & \eta_- \end{pmatrix}, \quad (5)$$

where $\eta_\pm = \cos(2q_B l_B)[1 + \cos(2\phi_B)] \pm \sin(2q_B l_B)\sin(2\phi_B)$. Obviously, under the resonance conditions of $q_A l_A = -q_B l_B = n\pi/2$ ($n = 0, \pm 1, \cdots$), we have $M_{BB} = (-1)^n I$. Meanwhile, the second pair of matrices "$M_A M_A$" comes to the center of M. Again, if the resonance conditions are satisfied, $M_{AA} = M_A M_A = (-1)^n I$ holds. Repeating the same pairing procedure, the total transfer matrix becomes $M = I$, which results in the perfect transmission with $T = 1$. Therefore, the mirror symmetry in the DGSL can indeed generate a dimerlike positional correlation, and this kind of positional correlation leads to the emergence of extra DPs. Corresponding to the DPs, the perfect transmissions are obtained at the resonant modes of DGSL.

Based on the above analysis, we numerically study the electronic dispersion relation for the DGSL of *ABBA*. The electronic dispersion relation for the PGSL of *ABAB* has also been calculated for comparison. Figure 1 shows the electronic band structures with the electrostatic potential $V_A = 60$ meV, $V_B = 0$ meV, and the potential width are set as $W = l_A = l_B = 50$ nm. It is shown in Fig. 1(a) that one DP is formed in the zero-$\bar{k}$ gap of PGSL. This feature is actually the same as that in several recent works,[14–18] and it is not the emphasis of the present work. It should be noted that a pair of extra DPs are induced in the zero-$\bar{k}$ gap of DGSL [Fig. 1(b)]. The induced DPs are lacked in the band structure of PGSL. This feature originates from the mirror symmetry of the dimerlike potential in the DGSL. Due to this kind of positional correlation, the condition for the emergence of DPs becomes $q_A l_A = -q_B l_B = n\pi/2$ ($n = 0, \pm 1, \cdots$) in the DGSL. That means the phase difference of incident waves through each element A (B) is an integer multiple of $\pi/2$ for the appearance of DPs in the DGSL. However, the condition for the appearance of DPs in the PGSL is that the phase difference of incident waves across each element A (B) should be an integer multiple of π. As a result, when the phase difference of incident waves across each element A (B) is a half-integer multiple of π, extra DPs can be obtained in the

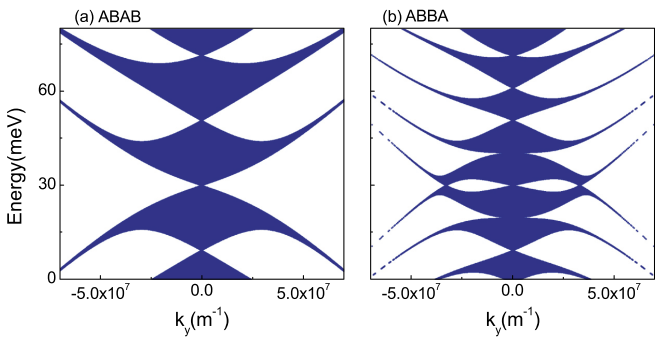

FIG. 1. The electronic band structures for (a) PGSL of *ABAB* and (b) DGSL of *ABBA*, with $V_A = 60$ meV, $V_B = 0$ meV, and $W = 50$ nm.

DGSL. Therefore, extra DPs, which do not exist in the PGSL, emerge in the DGSL due to the mirror symmetry of dimerlike positional correlations of the system.

It is necessary to pay attention to the electronic dispersion relation when the repeated number of units m is changed in the DGSL of $S(m) = (AB)^m(BA)^m$. As shown in Figs. 2(a) and 2(b), the energy levels tend to repel each other, and the band splits into sub-band at inclined incidence as m is enhanced. In other words, more and more energy gaps are opened when $k_y \neq 0$ by increasing m. However, the number and the position of DPs in zero-$\bar{k}$ gap are not changed. Then, the variation of m does not affect the DPs in the zero-$\bar{k}$ gap of DGSL. On the other hand, if we increase the potential width, more and more DPs appear in the zero-$\bar{k}$ gap of DGSL. For example, there exist five DPs within the zero-$\bar{k}$ gap when $W = 90$ nm [Fig. 2(c)], and seven DPs occur in the zero-$\bar{k}$ gap when $W = 120$ nm [Fig. 2(d)]. Therefore, multiple DPs can be obtained in the zero-$\bar{k}$ gap of DGSL by tuning the potential width of the system.

Now we consider the transmission of electrons in the DGSL. Figure 3 shows the transmission coefficient as functions of incident energy and incident angle in the DGSL with $m = 1$ and different potential width W. As shown in Fig. 3(a), the contour plot of perfect transmission is reminiscent of the letter "V." We find that the tip of "V" locate at the energy $E = 30$ meV which corresponds to the zero-$\bar{k}$. Around this energy, a node of perfect transmission is observed at normal incidence. While the contour plot of perfect transmission opens under the inclined incident angles. The perfect transmission at normal incidence results from the chirality of the carriers which prevents them from being reflected by the barriers in DGSL. By increasing W, the continuous range of perfect transmission is reduced by "inserting" small gaps between regions of perfect transmission [Figs. 3(b)–3(d)]. In the zero-$\bar{k}$ gap, the contour plots of perfect transmission gradually touch together and form nodes of perfect transmission at inclined angles when the potential width is enlarged. Specifically, there exist two nodes of perfect transmission in the zero-$\bar{k}$ gap of DGSL with $W = 50$ nm [Fig. 3(b)], three nodes of perfect transmission with $W = 90$ nm [Fig. 3(c)], and four nodes of perfect transmission with $W = 120$ nm [Fig. 3(d)], respectively. This is physically understandable due to the formation of DPs in the electronic band structure when the potential width is increased in the DGSL. Whenever there is a DP, there is the resonant transmission correspondingly. Therefore, multiple resonant transmissions are obtained in the zero-$\bar{k}$ gap by increasing the width of modulation potential in the DGSL.

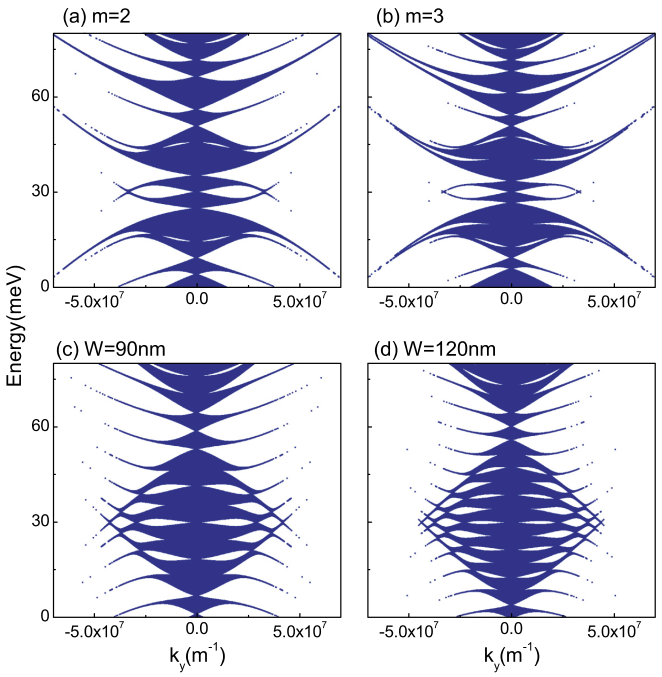

FIG. 2. (a) and (b) Electronic band structures in the DGSL of $S(m) = (AB)^m(BA)^m$ with $W = 50$ nm and different m: (a) $m = 2$; (b) $m = 3$, respectively. (c) and (d) The electronic band structures of DGSL with $m = 1$ and different potential width: (c) $W = 90$ nm; (d) $W = 120$ nm, respectively. The potentials in DGSL have been set as $V_A = 60$ meV and $V_B = 0$ meV.

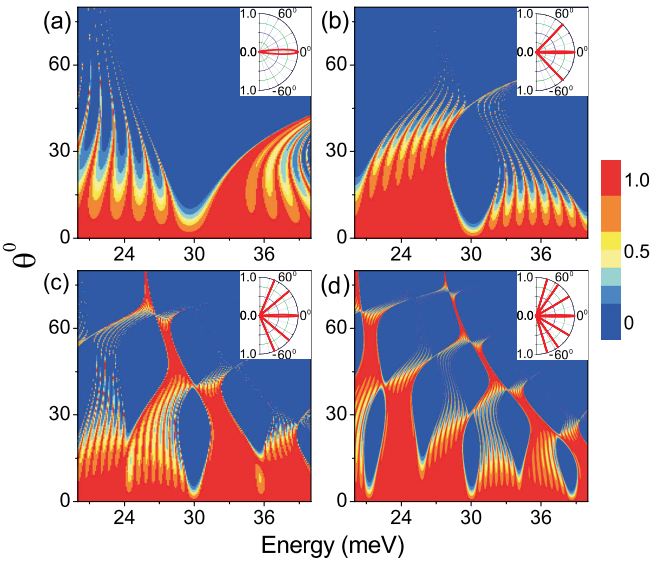

FIG. 3. (a)–(d) The contour plot of the transmission coefficient as functions of incident energy and incident angle in the DGSL with $m = 1$, $V_A = 60$ meV, $V_B = 0$ meV, and different potential width: (a) $W = 30$ nm, (b) $W = 50$ nm, (c) $W = 90$ nm, and (d) $W = 120$ nm, respectively. The insets present the transmission coefficient against the incident angle when $E = 30$ meV.

There is another way to demonstrate the behavior of perfect transmission in DGSL. In the insets of Figs. 3(a)–3(d), we have calculated the transmission coefficient against the incident angles of carriers for several values of the potential width W, while the incident energy is set as $E = 30$ meV. Obviously, resonant transmissions with $T = 1$ are observed in the insets of Figs. 3(a)–3(d). When $W = 30$ nm, there is only one resonant transmission peak located at 0^0 [the inset of Fig. 3(a)]. By increasing W, more and more resonant peaks appear symmetrically on both sides of the 0° resonant peak. For example, there are three resonant peaks located at 0^0 and $\pm 46.3^0$ when $W = 50$ nm [the inset of Fig. 3(b)]; five resonant peaks occurred at 0^0, $\pm 39.9^0$, $\pm 67.4^0$ when $W = 90$ nm [the inset of Fig. 3(c)]; seven resonant peaks emerged at 0^0, $\pm 30.4^0$, $\pm 54.9^0$, $\pm 73.3^0$ when $W = 120$ nm [the inset of Fig. 3(d)]. Thereafter, transmission coefficient can be changed rapidly from one to zero or from zero to one by modulating the incident angles of carriers in the DGSL. This feature provides a way of electron filtering and may have potential application in the designing of filtering devices.

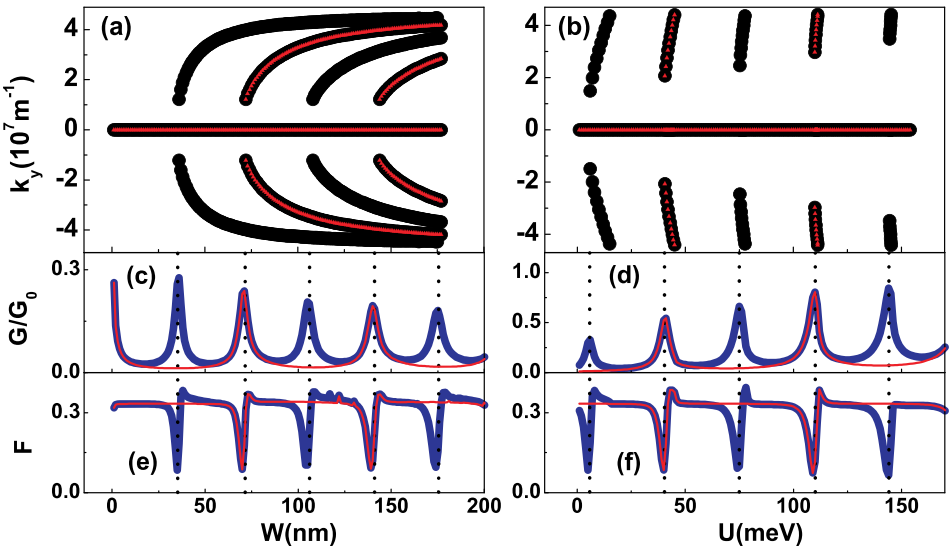

FIG. 4. (a) and (b) The distribution of DPs in k space for DGSL of *ABBA* with black circles and for PGSL of *ABAB* with red triangles. (c)–(f) The conductance (G/G_0) and Fano factor (F) for DGSL of *ABBA* with thick blue lines and for PGSL of *ABAB* with thin red lines. The vertical dotted lines indicate the location of resonant peaks. (a) Distribution of DPs in k space, (c) conductance, and (e) Fano factor versus W with $U = 0$ meV. (b) Distribution of DPs in k space, (d) conductance, and (f) Fano factor against U with $W = 30$ nm. The potential barrier A and well B are set as $V_A = (60 + U)$ meV and $V_B = (0\text{-}U)$ meV, respectively.

Due to the fact that the perfect transmissions are associated with the DPs, it is worthwhile to focus on the zero-$\bar{k}$ states or the DPs in the zero-$\bar{k}$ gap of DGSL. The black circles in Fig. 4(a) show the distribution of DPs in k space against the potential width W in the DGSL. Obviously, there are several critical values of W. By assuming $k_y = 0.01\,\text{nm}^{-1}$, we can get the critical values, i.e., $W_1 \approx 35.4$ nm, $W_2 \approx 70.8$ nm, $W_3 \approx 106.2$ nm, and $W_4 \approx 141.6$ nm, respectively. We find that there is only one DP located at $k_y = 0\,\text{nm}^{-1}$ when $W < W_1$. However, a pair of DPs appear when $W > W_1$. By increasing W, this pair of DPs move toward larger absolute values of k_y. The second pair of DPs emerge when $W > W_2$. Continuously, the third pair of DPs appear when $W > W_3$, and the fourth pair of DPs occur when $W > W_4$. On the other hand, the distribution of DPs in k space can also be manipulated by changing the amplitude of potentials in the DGSL. In order to manipulate the amplitude of potentials, we introduce an applied voltage on the barriers and wells in the DGSL. Then, the potential of barrier A is reset as $V_A = (60 + U)$ meV, and the potential of well B is reset as $V_B = (0\text{-}U)$ meV, respectively. The black circles in Fig. 4(b) present the distribution of DPs in k space against modulation potential U in the DGSL. Similarly, there are the critical values of U. With $k_y = 0.01\,\text{nm}^{-1}$, the critical values are obtained as $U_1 \approx 5.2$ meV, $U_2 \approx 39.4$ meV, $U_3 \approx 73.8$ meV, $U_3 \approx 73.8$ meV, and $U_4 \approx 108.3$ meV, respectively. Obviously, there exists only one DP located at $k_y = 0\,\text{nm}^{-1}$ when $U < U_1$. With $U > U_1$, the first pair of DPs emerge in the zero-$\bar{k}$ gap of DGSL. However, this pair of DPs processed rapidly apart from $k_y = 0\,\text{nm}^{-1}$ by increasing U. Subsequently, they disappear when U approaches the next critical value of U_2. Afterwards, the second pair of DPs emerge when $U > U_2$. Different from the first pair of DPs, the second pair of DPs process more rapidly toward large absolute values of k_y. As a consequence, they are vanished before the third pair of DPs appear with $U > U_3$. It is found that the more large value of U, the more rapid process of DPs in k space of DGSL. In Figs. 4(a) and 4(b), we also present the distribution of DPs for PGSL with red triangles. It is obvious that the branches of DPs for PGSL overlap with the branches for DGSL alternately. Therefore, extra DPs, which are missed in the PGSL, are observed in the zero-$\bar{k}$ gap of DGSL. One can manipulate the number and position of DPs in the zero-$\bar{k}$ gap by tuning the width or the amplitude of potentials in the DGSL.

It is worthwhile to investigate the conductance and the Fano factor of the system. The thick blue line in Fig. 4(c) presents the conductance as a function of the potential width at the incident energy $E = 30$ meV in the DGSL. It is shown that the conductance oscillates against the potential width W. Interestingly, these resonant peaks occur accompanying with the emergence of DPs. For example, the first resonant peak appears near W_1, the second resonant peak occur around W_2, and so on in the DGSL. On the other hand, the resonance of conductance can also be manipulated by the modulation potential U. The thick blue line in Fig. 4(d) shows the conductance against U in the DGSL. It is clear that the conductance resonates with the modulation potential U. Also, the resonant peaks against U occur accompanying with the emergence of DPs. For instance, the first resonant peak appears around U_1, the second resonant peak occurs near U_2, and the like in the DGSL. However, between the peaks the overall scale increases by enhancing U [Fig. 4(d)]. Therefore, the dimerlike potential on graphene tends to enhance the conductance of the system. For comparison, the conductance for PGSL is plotted with thin red lines in Figs. 4(c) and 4(d). It is shown that the resonant peaks of conductance for PGSL are coincided with the peaks for DGSL alternatively. Between these peaks, extra resonant peaks of conductance are observed for DGSL. This feature comes from the mirror symmetry of the dimerlike potential in the DGSL, which can induce extra DPs. Accompanying with the emergence of the induced DPs, extra resonant peaks of conductance occur in the DGSL. Moreover, the Fano factor (F) against W and U are also depicted in Figs. 4(e) and 4(f) with thick blue lines for DGSL and thin red lines for PGSL. It is demonstrated that F is approximately equal to 1/3 except the resonant points. At the resonant points, F tends to zero. That means the system behaves diffusively and the conductance is well defined apart from some resonances. The resonances of

conductance may be as a direct experimental signature of the presence of DPs. Extra resonant peaks of conductance can be observed accompanying with the emergence of the induced DPs in the DGSL.

In summary, extra DPs have been obtained in the zero-$\bar{k}$ gap of DGSL. One can manipulate the number and position of DPs in the zero-$\bar{k}$ gap by tuning the width or the amplitude of the potentials in the DGSL. Correspondingly, multiple perfect transmissions are observed at the resonant modes. Moreover, the conductance for DGSL presents extra resonant peaks accompanying with the emergence of the induced DPs. The investigations may have potential applications in graphene-based electronic devices.

This work was supported by grants from the National Natural Science Foundation of China (Grant Nos. 10904061, 11034005, 61077023, 11021403, and 50977042), the State Key Program for Basic Research from the Ministry of Science and Technology of China (Grant Nos. 2012CB921502 and 2010CB630705), and partly by the Ministry of Education of China (Grant No. 20100091110029).

[1]K. S. Novoselov, A. K. Geim, S. V. Morozov, D. Jiang, Y. Zhang, S. V. Dubonos, I. V. Grigorieva, and A. A. Firsov, Science **306**, 666 (2004).
[2]C. W. J. Beenakker, Rev. Mod. Phys. **80**, 1337 (2008); A. H. C. Neto, F. Guinea, N. M. R. Peres, K. S. Novoselov, and A. K. Geim, *ibid.* **81**, 109 (2009).
[3]K. S. Novoselov, A. K. Geim, S. V. Morozov, D. Jiang, M. I. Katsnelson, I. V. Grigorieva, S. V. Dubonos, and A. A. Firsov, Nature (London) **438**, 197 (2005); Y. Zhang, Y. W. Tan, H. L. Stormer, and P. Kim, *ibid.* **438**, 201 (2005).
[4]V. P. Gusynin and S. G. Sharapov, Phys. Rev. Lett. **95**, 146801 (2005).
[5]M. I. Katsnelson, K. S. Novoselov, and A. K. Geim, Nat. Phys. **2**, 620 (2006).
[6]N. Stander, B. Huard, and D. Goldhaber-Gordon, Phys. Rev. Lett. **102**, 026807 (2009); A. F. Young and P. Kim, Nat. Phys. **5**, 222 (2009).
[7]C. Bai and X. Zhang, Phys. Rev. B **76**, 075430 (2007).
[8]B. Huard, J. A. Sulpizio, N. Stander, K. Todd, B. Yang, and D. Goldhaber-Gordon, Phys. Rev. Lett. **98**, 236803 (2007).
[9]J. C. Meyer, C. O. Girit, M. P. Crommie, and A. Zettl, Appl. Phys. Lett. **92**, 123110 (2008).
[10]A. L. V. de Parga, F. Calleja, B. Borca, M. C. G. Passeggi, Jr., J. J. Hinarejos, F. Guinea, and R. Miranda, Phys. Rev. Lett. **100**, 056807 (2008).
[11]Z. Sun, C. L. Pint, D. C. Marcano, C. Zhang, J. Yao, G. Ruan, Z. Yan, Yu Zhu, R. H. Hauge, and J. M. Tour, Nature Commun. **2**, 559 (2011).
[12]C.-H. Park, L. Yang, Y.-W. Son, M. L. Cohen, and S. G. Louie, Nat. Phys. **4**, 213 (2008).
[13]L. Brey and H. A. Fertig, Phys. Rev. Lett. **103**, 046809 (2009).
[14]C.-H. Park, Y.-W. Son, L. Yang, M. L. Cohen, and S. G. Louie, Phys. Rev. Lett. **103**, 046808 (2009).
[15]L.-G. Wang and S.-Y. Zhu, Phys. Rev. B **81**, 205444 (2010).
[16]Y. P. Bliokh, V. Freilikher, S. Savel'ev, and F. Nori, Phys. Rev. B **79**, 075123 (2009).
[17]M. Barbier, P. Vasilopoulos, and F. M. Peeters, Phys. Rev. B **81**, 075438 (2010).
[18]T. Ma, C. Liang, L.-G. Wang, and H.-Q. Lin, Appl. Phys. Lett. **100**, 252402 (2012); H. Huang, D. Liu, H. Zhang, and X. Kong, J. Appl. Phys. **113**, 043702 (2013).
[19]P.-L. Zhao and X. Chen, Appl. Phys. Lett. **99**, 182108 (2011).
[20]N. Abedpour, A. Esmailpour, R. Asgari, and M. R. R. Tabar, Phys. Rev. B **79**, 165412 (2009).
[21]D. H. Dunlap, H.-L. Wu, and P. W. Phillips, Phys. Rev. Lett. **65**, 88 (1990).
[22]V. Bellani, E. Diez, R. Hey, L. Toni, L. Tarricone, G. B. Parravicini, F. Domínguez-Adame, and R. Gómez-Alcalá, Phys. Rev. Lett. **82**, 2159 (1999).
[23]R. W. Peng, Y. M. Liu, X. Q. Huang, F. Qiu, Mu Wang, A. Hu, S. S. Jiang, D. Feng, L. Z. Ouyang, and J. Zou, Phys. Rev. B **69**, 165109 (2004); Z. Zhao, F. Gao, R. W. Peng, L. S. Cao, D. Li, Z. Wang, X. P. Hao, Mu Wang, and C. Ferrari, *ibid.* **75**, 165117 (2007).
[24]S. Datta, *Electronic Transport in Mesoscopic Systems* (Cambridge University Press, London, 1995); Y. Imry and R. Landauer, Rev. Mod. Phys. **71**, S306 (1999).